Am J Cancer Res 2026;16(3):813-824
www.ajcr.us /ISSN:2156-6976/ajcr0169845

Original Article

Isobavachalcone induces concurrent apoptosis and pyroptosis in anaplastic thyroid cancer cells by modulating the caspase-mediated cleavage of PARP and GSDME

Chuanming Zheng[1,2,5,6,7*], Aoni Zhou[3*], Lingling Ding[4*], Qiang Geng[2], Yanran Wang[2], Xiujuan Fan[2], Shiqian Wu[2], Ludan Zheng[2], Minghua Ge[1,2,5,6,7], Guowan Zheng[2,5,6]

[1]The Second School of Clinical Medicine, Zhejiang Chinese Medical University, Hangzhou 310053, Zhejiang, China; [2]Otolaryngology & Head and Neck Center, Cancer Center, Department of Head and Neck Surgery, Zhejiang Provincial People's Hospital (Affiliated People's Hospital), Hangzhou Medical College, 158 Shangtang Road, Hangzhou 310014, Zhejiang, China; [3]The Second School of Clinical Medicine, Hangzhou Normal University, Hangzhou 310018, Zhejiang, China; [4]Department of Otolaryngology-Head and Neck Surgery, The Affiliated Lihuili Hospital, Ningbo University, Ningbo 315040, Zhejiang, China; [5]Zhejiang Provincial Clinical Research Center for Head and Neck Cancer, Hangzhou 310014, Zhejiang, China; [6]Zhejiang Key Laboratory of Precision Medicine Research on Head and Neck Cancer, Hangzhou 310014, Zhejiang, China; [7]Postgraduate Training Base Alliance of Wenzhou Medical University (Zhejiang Provincial People's Hospital), Wenzhou 325000, Zhejiang, China. [*]Equal contributors.

Received November 7, 2025; Accepted March 6, 2026; Epub March 15, 2026; Published March 30, 2026

Abstract: Anaplastic thyroid carcinoma (ATC) is a highly lethal malignant tumor, and there's still no effective treatment for it. Isobavachalcone (IBC) is a chalcone derivative and comes from the traditional Chinese herb *Psoralea corylifolia*. IBC exhibits potent anti-cancer activity against various cancers. However, its efficacy and mechanism of action in ATC remain unclear. This research used *in vitro* and *in vivo* models to evaluate the anti-cancer effects of IBC on ATC. The results showed that IBC has significant anti-cancer effects with extremely low toxicity. Mechanically, IBC inhibits ATC cell growth by inducing cell cycle arrest in the G2/M and S phases. IBC induces apoptosis and pyroptosis, with caspase-dependent Poly ADP-ribose Polymerase (PARP) and Gasdermin E (GSDME) cleavage simultaneously. This study reveals a novel function of IBC in inducing pyroptosis in tumor cells, expands its known pharmacological spectrum and highlights its value as a therapeutic agent for ATC.

Keywords: Anaplastic thyroid carcinoma (ATC), isobavachalcone (IBC), pyroptosis, apoptosis

Introduction

Anaplastic thyroid carcinoma (ATC) is one of the most aggressive and lethal forms of thyroid cancer. Its 5-year survival rate is less than 7% and it causes over 50% of deaths related to thyroid cancer [1]. ATC is characterized by an aggressive clinical course, early metastasis, and poor responsiveness to conventional radiotherapy, chemotherapy, and targeted therapies. Currently, no curative standard therapy exists for ATC. The median survival time of ATC patients is just 4-10 months [1]. The prognosis of ATC remains very poor. Thus, there is an urgent need to develop novel drugs and effective treatments.

In recent years, traditional Chinese medicine's active ingredients have gotten more and more attention as anti-cancer drugs. This is because they have multi-target effects and are relatively less toxic. Isobavachalcone (IBC), a chalcone derivative from *Psoralea corylifolia*, is seen as a possible drug with broad-spectrum antitumor ability [2, 3]. IBC has demonstrated broad-spectrum antitumor efficacy against multiple cancer types, including colorectal, ovarian, lung, breast, gastric cancers, and squamous

cell carcinoma of the tongue. Its way of working involves inducing cell death, inhibiting cell proliferation, regulating oxidative stress, and modulating key signaling pathways [4-7]. In a colorectal cancer (CRC) model, IBC suppresses cell proliferation and colony formation in a dose- and time-dependent manner. Mechanistically, its ability to promote cell death includes nuclear morphological alterations, disruption of mitochondrial homeostasis (including an altered Bax/Bcl-2 balance and loss of mitochondrial membrane potential), enhanced cleavage of caspase-3 and PARP, and suppression of anti-apoptotic proteins XIAP and surviving [8]. In prostate cancer, IBC enhances its antitumor effects by modulating oxidative stress. Mechanistic studies have shown that IBC targets the selenocysteine-containing antioxidant enzyme thioredoxin reductase 1 (TrxR1), inhibiting its activity and leading excessive accumulation of reactive oxygen species (ROS). This ROS overload subsequently triggers endoplasmic reticulum (ER) stress and induces mitochondria-mediated apoptosis [9]. In summary, these findings suggest that induction of apoptosis is the main mechanism of IBC's antitumor activity. However, whether IBC possesses potent antitumor activity against ATC and its mechanism of action remains unclear.

Pyroptosis has emerged as a novel and promising therapeutic strategy for cancer treatment [10]. Compared with apoptosis, pyroptosis is a distinct form of programmed cell death characterized by strong inflammatory responses and immune activation, promoting the release and presentation of tumor-related antigens [11-13]. This process can remodel the immunosuppressive tumor microenvironment and reactivate immune surveillance, ultimately facilitating the elimination of tumor cells [14-17]. Different strategies and compounds have been reported to induce pyroptosis, including chemotherapeutic drugs, targeted inhibitors, and small - molecule modulators of gasdermin and inflammasomes [18-20]. Our previous studies have demonstrated that inducing pyroptosis in ATC cells effectively suppresses tumor growth [21-23]. Therefore, investigating whether IBC can induce pyroptosis in ATC cells is crucial for evaluating its potential as a novel and effective treatment for ATC.

In this study, we show that IBC exhibited potent anti-tumor activity against ATC cells *in vitro* and significantly suppressed tumor growth *in vivo*. IBC induces cell-cycle arrest at the G2/M and S phases, subsequently triggering both apoptosis and pyroptosis. This process involves caspase-dependent cleavage of PARP and GSDME. These findings show that IBC can induce pyroptosis in tumor cells, broaden our understanding of its pharmacological actions, and highlight its potential as an effective therapeutic option for ATC.

Materials and methods

Reagents and antibodies

Isobavachalcone (IBC with purity ≥ 99.50%) was purchased from Targetmol (#T3861, China), and dissolved in Dimethyl Sulfoxide (DMSO) which was diluted in the Roswell Park Memorial Institute 1640 (RPMI-1640) medium to a desired concentration. N-acetyl-L-cysteine (NAC, #S0077) was purchased from the Beyotime Institute of Biotechnology, China, while N-Benzyloxycarbonyl-Val-Ala-Asp-fluoromethyl ketone (Z-VAD-FMK) (#A1902) was purchased from ApexBio, USA. Polyethylene Glycol 300 (PEG300) (#T7022) and Tween 80 (#T13947) were obtained from Targetmol, China while goat anti-rabbit (#A0208) and anti-mouse (#A0216) HRP IgG secondary antibodies were purchased from Beyotime Institute of Biotechnology, China. Anti-PARP (#9532), anti-caspase-8 (#D35G2), anti-caspase 9 (#9502), and anti-cyclin B1 (#12231) antibodies were acquired from Cell Signaling Technology, USA, while anti-GAPDH (#60004-1-Ig) antibodies were purchased from Proteintech, China. Anti-GSDME (#ab215191), anti-cleaved caspase 9 (#ab23-24), and anti-caspase 3 (#ab32351) antibodies were purchased from Abcam, USA, while anti-Cyclin-dependent kinase 1 (anti-CDK1) (#ET1607-51), anti-cleaved-PARP (#ET1608-10) and anti-active caspase 3 (#ET-1602-47) were purchased from HuaAn Biotechnology, China.

Cell culture

The human ATC cell lines KHM-5M, KMH-2, C643, and CAL-62 were acquired from the National Infrastructure of Cell Line Resource (Shanghai, China). The 8505C cell line was procured from the Deutsche Sammlung von Mikroorganismen und Zellkulturen (DSMZ). All cell lines were cultured in RPMI-1640 medium containing 10% fetal bovine serum (FBS,

#KC001-01, KEL Biotech, USA) and 1% penicillin/streptomycin and maintained at 37°C in a humidified incubator. Prior to experimental treatments, cells were allowed to reach approximately 85% confluence.

Cell viability and colony formation assay

Cell viability was assessed using the Cell Counting Kit-8 (CCK-8, #K1018, ApexBio, USA). Cells were seeded in 96-well plates at a density of 4,000 cells per well and allowed to adhere for 24 hours in a 37°C, 5% CO_2 incubator. The control group received a vehicle containing DMSO at a final concentration of ≤ 0.1%. Following treatment, 10 μL of CCK-8 reagent and 90 μL of fresh RPMI-1640 medium supplemented with 10% FBS were added to each well. The plates were incubated for an additional 2 hours at 37°C, after which the absorbance at 450 nm was measured with a Synergy LX multi-mode microplate reader (BioTek Instruments, USA). For the colony formation assay, 8505C and KHM-5M cells were plated in 12-well plates at densities of 1,000 or 2,000 cells per well and exposed to increasing concentrations of IBC (0, 40, 50, and 60 μM). After one week of culture at 37°C, the resulting colonies were fixed with ethanol, stained with 0.1% crystal violet, and quantified.

Cell cycle analysis and determination of cell death rate

Cell cycle distribution was analyzed using a commercial Cell Cycle Kit (Lianke Bio, China) according to the manufacturer's protocol. Briefly, 8505C and KHM-5M cells were seeded in 6-well plates at densities of 1.8×10^5 cells per well. After treatment, cells were collected, washed with Phosphate-Buffered Saline (PBS), and stained with a DNA staining solution containing permeabilization buffer for 30 minutes in the dark. Cell cycle analysis was performed on a Navios flow cytometer (Beckman Coulter, USA) at the lowest acquisition speed, and data were processed using FlowJo software.

Determination of cell death rate

Cell death was determined by Annexin V-FITC and PI kit (Lianke Bio, China) following the manufacturer's instructions. The 8505C and KHM-5M cells (1.8×10^5 cells/well) were seeded in 6-well plates and treated with different drugs after complete attachment. After 24 h of incubation at 37°C, both attached and the floating cells were harvested, washed twice in ice-cold PBS and then suspended with 1 × binding buffer. The cells were labeled with 1 μl Annexin V-FITC and 2 μl PI and then incubated in the dark for 5 min at room temperature. Apoptosis was analyzed by flow cytometer and the results were analyzed using Flowjo to assess cell death rate.

Quantification of extracellular dehydrogenase (LDH) and interleukin-1β (IL-1β) levels

Pyroptosis was evaluated by measuring the release of lactate LDH and IL-1β into the cell culture supernatant. Extracellular LDH activity was quantified using a commercial LDH assay kit (#C0016, Beyotime Biotechnology, China), while IL-1β levels were determined by an ELISA kit (MM-0181H1, Meimian, China) according to the respective manufacturers' instructions. Absorbance was measured at 450 nm.

Measurement of intracellular reactive oxygen species (ROS) levels

Intracellular Reactive Oxygen Species (ROS) levels were measured using the fluorescent probe DCFH-DA (2',7'-dichlorodihydrofluorescein diacetate, #T15458, TargetMol, China). Briefly, cells were loaded with 10 μM 2',7'-dichlorodihydrofluorescein diacetate (DCFH-DA) in serum-free RPMI-1640 medium and incubated in the dark at 37°C for 30 minutes. Following incubation, the cells were washed twice with serum-free medium to remove excess probe. The fluorescence intensity, corresponding to intracellular ROS levels, was then immediately quantified by flow cytometry.

Western blotting

After drug treatment, the cells were lysed on ice using Radioimmunoprecipitation Assay buffer (RIPA buffer) (#P0013, Beyotime, China) supplemented with Phenylmethylsulfonyl fluoride (PMSF). Protein concentrations were determined with a Bicinchoninic Acid Assay (BCA assay kit) (Thermo Fisher Scientific, USA). Equal amounts of protein were separated by Sodium Dodecyl Sulfate-PolyAcrylamide Gel Electrophoresis (SDS-PAGE) on 4-20% precast gels (#P0524M, Beyotime) and transferred to Polyvinylidene Fluoride (PVDF) membranes. After blocking with 5% non-fat milk in TBST, the

membranes were incubated with primary antibodies overnight at 4°C, followed by HRP-conjugated secondary antibodies for 1 hour at room temperature. Protein bands were visualized using an enhanced chemiluminescence (ECL) kit (#FD8020, Fdbio Science, China) and imaged with a ChemiDoc MP system (Bio-Rad, USA).

In vivo xenograft tumor model

An *in vivo* xenograft model was established by subcutaneously injecting 8505C cells (2×10^6 cells in 100 μL) into female BALB/c nude mice (3-4 weeks old, 16-20 g). One week post-inoculation, the mice were randomly assigned into three groups (n = 6 per group) and administered daily intraperitoneal injections for 12 days as follows: vehicle control (5% DMSO, 30% PEG300, 10% Tween-80, 55% PBS), IBC (10 mg/kg), or IBC (20 mg/kg). Tumor volumes and body weights were recorded daily. Tumor volume was calculated as 0.5 × (shortest diameter)^2 × (longest diameter). At the endpoint, mice were euthanized by cervical dislocation, and tumors and major organs (heart, liver, kidneys) were harvested for weight measurement and histopathological examination. Tissue samples were either fixed in 4% formalin for paraffin embedding or lysed for protein extraction. All animal procedures were approved by the Animal Ethics Committee of Zhejiang Provincial People's Hospital (Approval No. 20250914406417).

Immunohistochemistry

For immunohistochemistry, paraffin-embedded tissue sections were deparaffinized, subjected to antigen retrieval, and blocked with 3% H_2O_2. Sections were then incubated with primary antibodies overnight, followed by appropriate secondary antibodies and HRP-conjugated IgG. Signal development was performed using DAB, and nuclei were counterstained with hematoxylin. Stained sections were scanned with a KF-PRO-005 slide scanner (Konfoong Biotech), and positive signals were identified as brown-yellow staining.

Statistical analysis

Data are presented as mean ± standard deviation (SD). Comparisons between two groups were performed using Student's t-test, while differences among multiple group sat a single time point were assessed by one-way analysis of variance (ANOVA). For longitudinal data involving a time variable, such as tumor growth curves and mouse body weight changes, two-way repeated measures ANOVA was employed to evaluate the differences between groups over time. A two-tailed *P*-value less than 0.05 was considered statistically significant. All statistical analyses were performed using GraphPad Prism 10 (GraphPad Software, USA).

Results

IBC inhibits ATC cell proliferation and colony formation, and induce cell cycle arrest

To assess the effect of IBC on ATC cell viability, the CCK-8 assay was performed. IBC significantly inhibited the viability of ATC cells in a dose-dependent manner, with IC_{50} values of 57.10 μM for 8505C, 51.10 μM for BHT-101, 65.27 μM for KHM-5M, 56.30 μM for C643, and 79.29 μM for Hth-7 cells (**Figure 1A**, **1B**). Furthermore, IBC significantly inhibited colony formation in a dose-dependent manner in both 8505C and KHM-5M cells (**Figure 1C**), consistent with its inhibitory effect on cell viability.

Flow cytometry analysis of cell cycle distribution showed that after 24 hours of IBC treatment, cell cycle arrest was significantly induced in both 8505C and KHM-5M cells, primarily occurring in the G2/M and S phase (**Figure 1D**, **1E**). Consistent with this, Western blot analysis revealed a significant downregulation of the G2/M phase-associated cyclin Cyclin B1 after 24 hours of IBC treatment (**Figure 1F**). Together, these results indicate that IBC inhibits ATC cell proliferation in part by inducing cell cycle arrest.

IBC simultaneously induces apoptosis and pyroptosis in ATC cells

We next looked into whether IBCs could cause ATC cell death because of their inhibitory effect on cell viability. IBCs dose-dependently induced apoptosis in 8505C and KHM-5M cells, as evidenced by an increase in the number of dead cells, according to flow cytometry analysis using FITC-Annexin V/PI staining (**Figure 2A**). Cell fragmentation into apoptotic bodies and other morphological changes consistent with apoptosis were further verified by bright-field

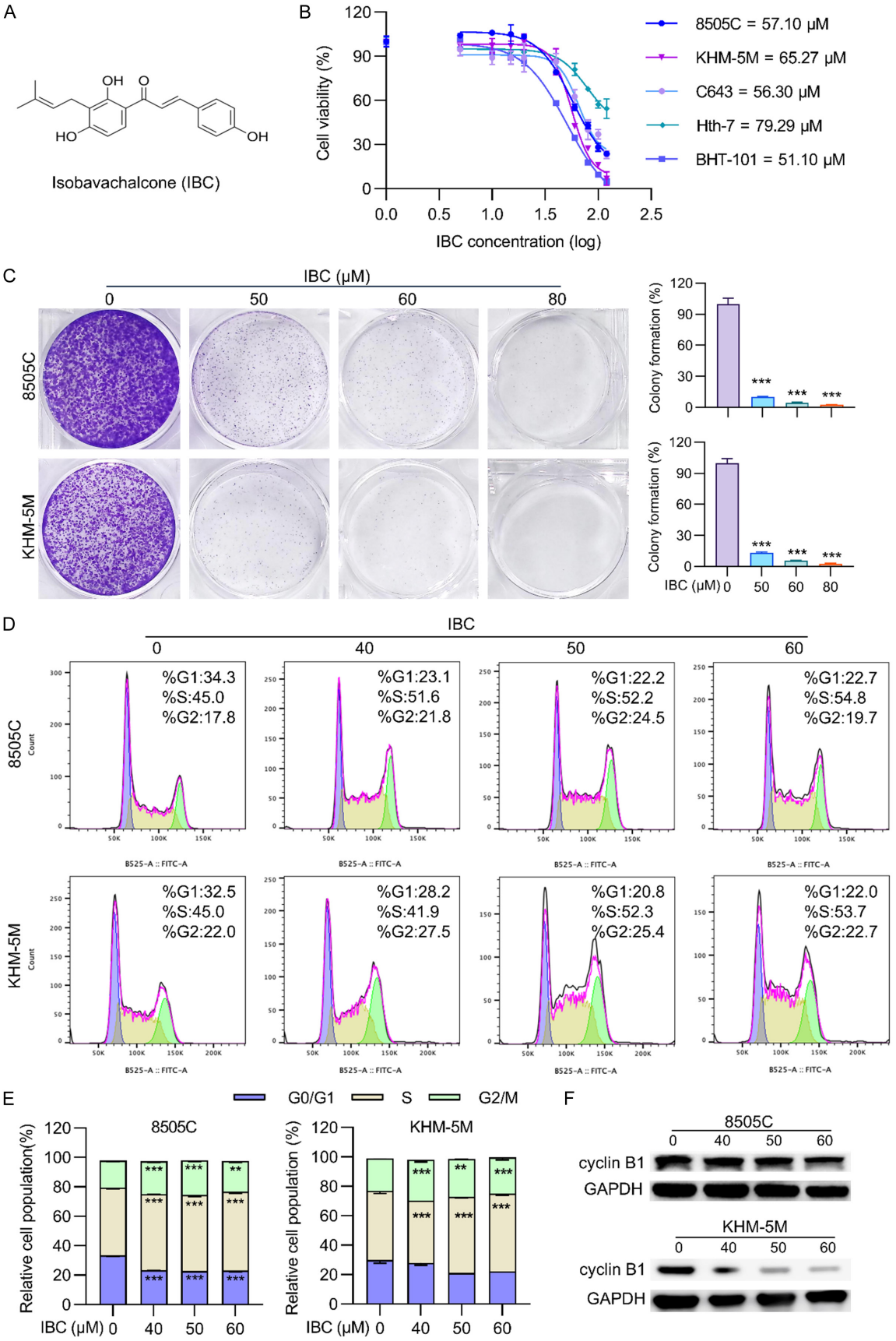
A
OH
O
HO
OH
Isobavachalcone (IBC)
B
Cell viability (%)
IBC concentration (log)
8505C = 57.10 μM
KHM-5M = 65.27 μM
C643 = 56.30 μM
Hth-7 = 79.29 μM
BHT-101 = 51.10 μM
C
IBC (μM)
0
50
60
80
8505C
KHM-5M
Colony formation (%)
***
D
IBC
0
40
50
60
8505C
KHM-5M
Count
%G1:34.3
%S:45.0
%G2:17.8
%G1:23.1
%S:51.6
%G2:21.8
%G1:22.2
%S:52.2
%G2:24.5
%G1:22.7
%S:54.8
%G2:19.7
%G1:32.5
%S:45.0
%G2:22.0
%G1:28.2
%S:41.9
%G2:27.5
%G1:20.8
%S:52.3
%G2:25.4
%G1:22.0
%S:53.7
%G2:22.7
B525-A :: FITC-A
E
G0/G1
S
G2/M
8505C
KHM-5M
Relative cell population(%)
IBC (μM) 0 40 50 60
F
8505C
cyclin B1
GAPDH
KHM-5M

Figure 1. IBC inhibits ATC cell proliferation, colony formation, and induces cell cycle arrest. (A) Compound IBC chemical formula is shown. (B) 8505C, KHM-5M, C643, Hth-7, and BHT-101 cells were exposed to varying IBC concentrations (0, 5, 10, 15, 20, 40, 60, 80, 100 and 120 μM) for 24 h. Cell viability was determined by the CCK-8 assay. IC_{50} values were calculated from non-linear regression plots using the GraphPad Prism 10 software. (C) Representative images of 8505C and KHM-5M cell clone formation at the indicated concentrations were quantified using the ImageJ software (n = 3). Cell cycle phase distribution of IBC-treated ATC cells (8505C and KHM-5M) for 12 h were determined by flow cytometry (D), the proportions of cell populations at each cell cycle phase relative to total phases (E), protein levels of cyclin B1 were measured by Western blot assays (F). Data are shown as mean ± SD for n = 3. **P < 0.01, ***P < 0.001.

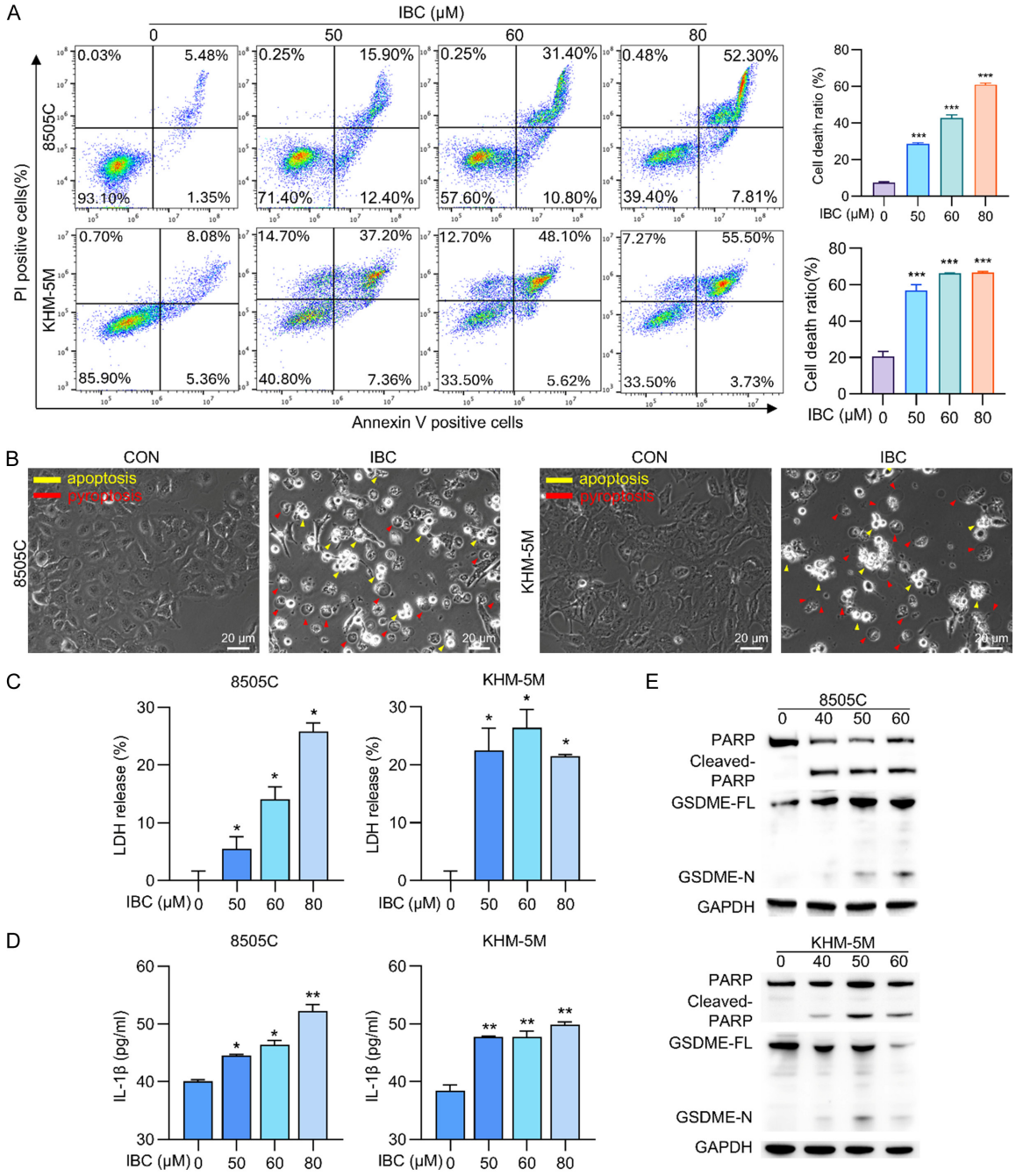

Figure 2. IBC induces apoptosis and pyroptosis in ATC cells. A. The ratio of cell death in 8505C and KHM-5M cultures increased after 24 hours of IBC treatment in a dose-dependent manner (0, 50, 60, and 80 μM), as assessed by flow cytometry. B. Following treatment with 60 μM IBC, 8505C and KHM-5M cells exhibited morphological changes char-

acteristic of apoptosis (yellow arrows) and pyroptosis (red arrows). C. LDH release in the culture medium was measured following 24-hour IBC treatment (0, 50, 60, and 80 μM) using a commercial assay kit. D. IL-1β concentration in the culture medium was measured following 24-hour IBC treatment (0, 50, 60, and 80 μM) using a commercial ELISA kit. E. The protein levels of full-length and cleaved forms of PARP, and GSDME in 8505C and KHM-5M cells were analyzed by western blotting after a 24-hour treatment with IBC (0, 40, 50, and 60 μM). Values are presented as mean ± SD for n = 3. *P < 0.05, **P < 0.01, ***P < 0.001.

phase-contrast microscopy (**Figure 2B**). In the meantime, we also noticed cell swelling that resembled bubbles (**Figure 2B**), a characteristic of pyroptosis. We further assessed pyroptosis by measuring the release of extracellular lactate dehydrogenase (LDH) and IL-1β. In ATC cells, IBC significantly increased extracellular LDH and IL-1β release in a dose-dependent manner (**Figure 2C**, **2D**), which is consistent with pyroptosis induction. In conclusion, these findings show that IBC causes ATC cells to undergo pyroptosis and apoptosis.

IBC-induced apoptosis and pyroptosis in ATC cells involve caspase-3-mediated PARP and GSDME cleavage

To elucidate the molecular mechanisms by which IBC induces apoptosis and pyroptosis, we examined apoptosis- and pyroptosis-related proteins. Western blot analysis showed that IBCs dose-dependently induced the cleavage of caspase-3 and PARP, as well as the cleavage of GSDME, a key pyroptosis mediator (**Figures 2E** and **3A**). Pretreatment with the pan-caspase inhibitor Z-VAD-FMK (Z-VAD) significantly and partially reversed IBC-induced ATC cell viability inhibition (**Figure 3B**) and partially reduced the number of dead cells (**Figure 3C**). Extracellular LDH release was also significantly reduced after Z-VAD treatment (**Figure 3D**). Western blot analysis confirmed that Z-VAD effectively inhibited the cleavage of caspase-3, PARP, and GSDME (**Figure 3E**). Collectively, these results indicate that IBC may induce ATC cell apoptosis partially via caspase-3-dependent PARP cleavage and pyroptosis potentially through GSDME cleavage.

IBC inhibits ATC xenograft growth in nude mice

To assess the *in vivo* antitumor efficacy and safety of IBC, a subcutaneous ATC xenograft model was established in BALB/c nude mice using 8505C cells. Once tumors were established, mice were treated with intraperitoneal injections of IBC. IBC significantly inhibited tumor growth in a dose-dependent manner, without causing significant changes in body weight across the treatment groups (**Figure 4A-D**). H&E staining of tumor tissues revealed a looser tissue architecture in IBC-treated tumors (**Figure 4E**). Immunohistochemistry showed a significant decrease in Ki-67 expression and a concomitant increase in cleaved caspase-3 and cleaved PARP levels compared with controls (**Figure 4F**). Serum biochemical assays showed no significant changes in ALT, AST, CR, UA, ALB, ALP, and BUN (**Figure 4G**), indicating that IBC did not compromise liver or kidney function. Histological analysis of major organs (heart, liver, kidney and spleen) by H&E staining revealed no obvious pathological alterations (**Figure 5**). These data collectively demonstrate that IBC induces apoptosis and pyroptosis *in vivo* and inhibits the growth of ATC xenograft tumors, consistent with its *in vitro* activity.

Discussion

Isobavachalcone (IBC) is the main active ingredient of the traditional Chinese medicine *Psoralea corylifolia* and belongs to the chalcone class of compounds [24]. IBC has been reported to have a wide range of pharmacological activities, including anti-inflammatory, antioxidant and antitumor effects [2, 4]. In terms of anti-tumor activity, IBC has been shown to possess broad-spectrum anti-tumor activity, including breast cancer, hepatocellular carcinoma and colorectal cancer [5, 25, 26]; however, its activity against highly aggressive ATC has not been systematically studied. Given the extremely high malignancy, short survival time and lack of effective treatment for ATC, exploring the antitumor potential of IBC and elucidating its mechanism of action has important translational medical significance. Our study shows that IBC exhibits potent antitumor activity against ATC both *in vitro* and *in vivo*, and has no detectable effect on the body weight or major organs of mice, indicating good safety. These findings suggest that IBC is a promising candidate for ATC therapy.

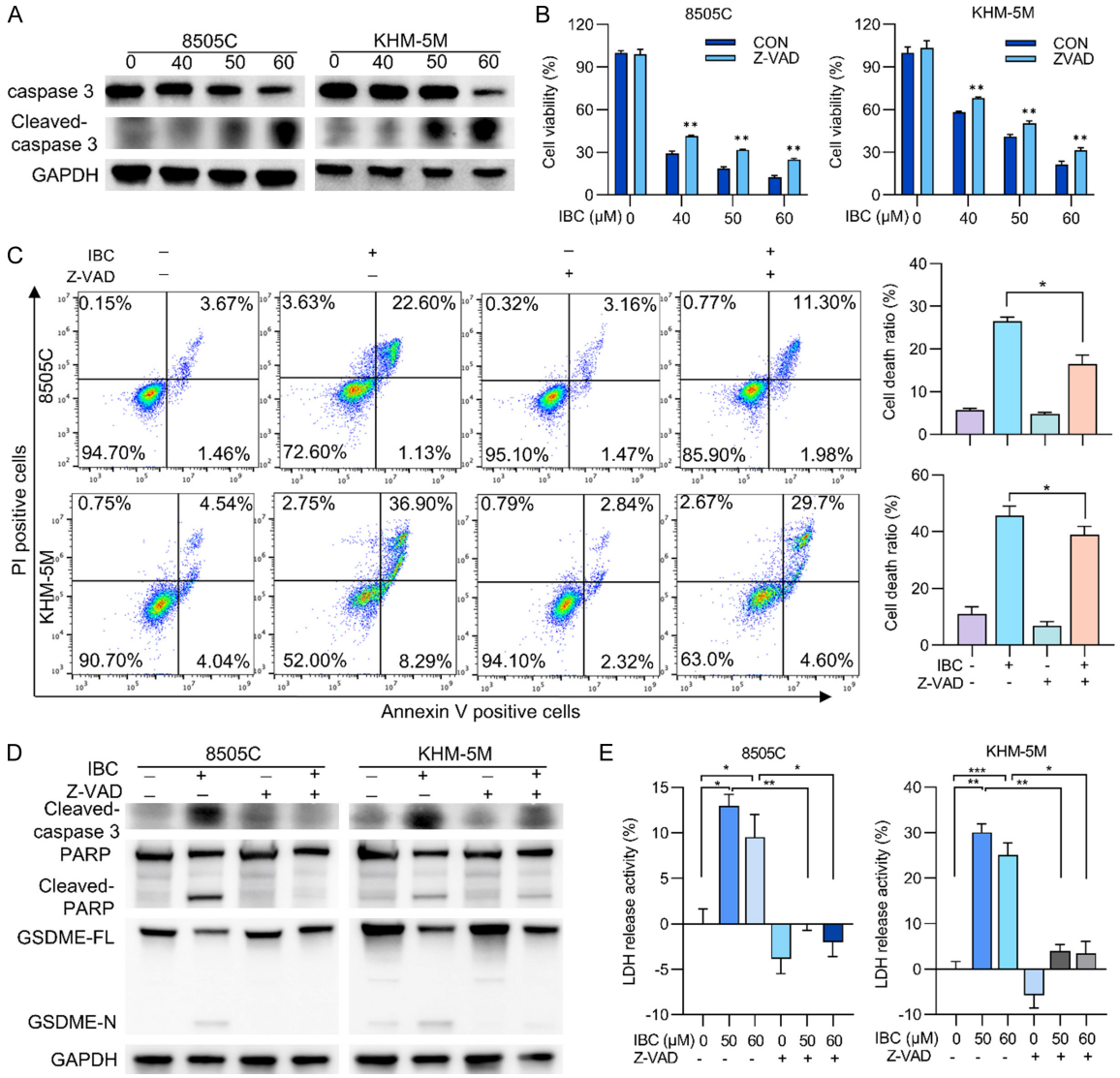

Figure 3. Caspase-3 mediates IBC-induced PARP-dependent apoptosis and GSDME-dependent pyroptosis. (A) The protein levels of full-length and cleaved forms of caspase 3 in 8505C and KHM-5M cells were analyzed by western blotting after a 24-hour treatment with IBC (0, 40, 50, and 60 μM). (B) The viability of 8505C and KHM-5M cells was determined by CCK-8 assay following 24 h exposure to IBC (0, 40, 50, 60, and 80 μM), with or without a 2 h pretreatment with the caspase inhibitor Z-VAD (20 μM), while cell death was assessed by flow cytometry and the ratio presented (C). Following a 24-hour treatment with IBC (0, 50, 60 μM) with or without Z-VAD (20 μM), the cleavage of PARP, caspase-3, and GSDME was assessed by western blot analysis (D), and LDH release into the culture supernatant was quantified using an LDH assay kit (E). Values are shown as mean ± SD for n = 3. ns $P > 0.05$, *$P < 0.05$, **$P < 0.01$, ***$P < 0.001$.

Pyroptosis is a form of programmed cell death resembling necrosis, mediated by gasdermin family proteins such as GSDMD and GSDME. It is characterized by cell swelling, plasma membrane rupture, and the release of pro-inflammatory cytokines, including IL-1β and IL-18 [10, 12, 27]. This inflammatory form of cell death can trigger a robust antitumor immune response [28-30]. In tumor cells, caspase-3 cleaves GSDME, releasing its N-terminal fragment, which forms pores in the membrane and triggers pyroptosis [31]. Tumor cells with low GSDME expression tend to undergo apoptosis rather than pyroptosis [32, 33]. Pyroptosis exposes tumor antigens and releases inflammatory mediators, alleviating immunosuppression in the tumor microenvironment and potentially enhancing immunotherapy efficacy [34, 35]. In clinical studies, promoter methylation-mediated silencing of GSDME has been detect-

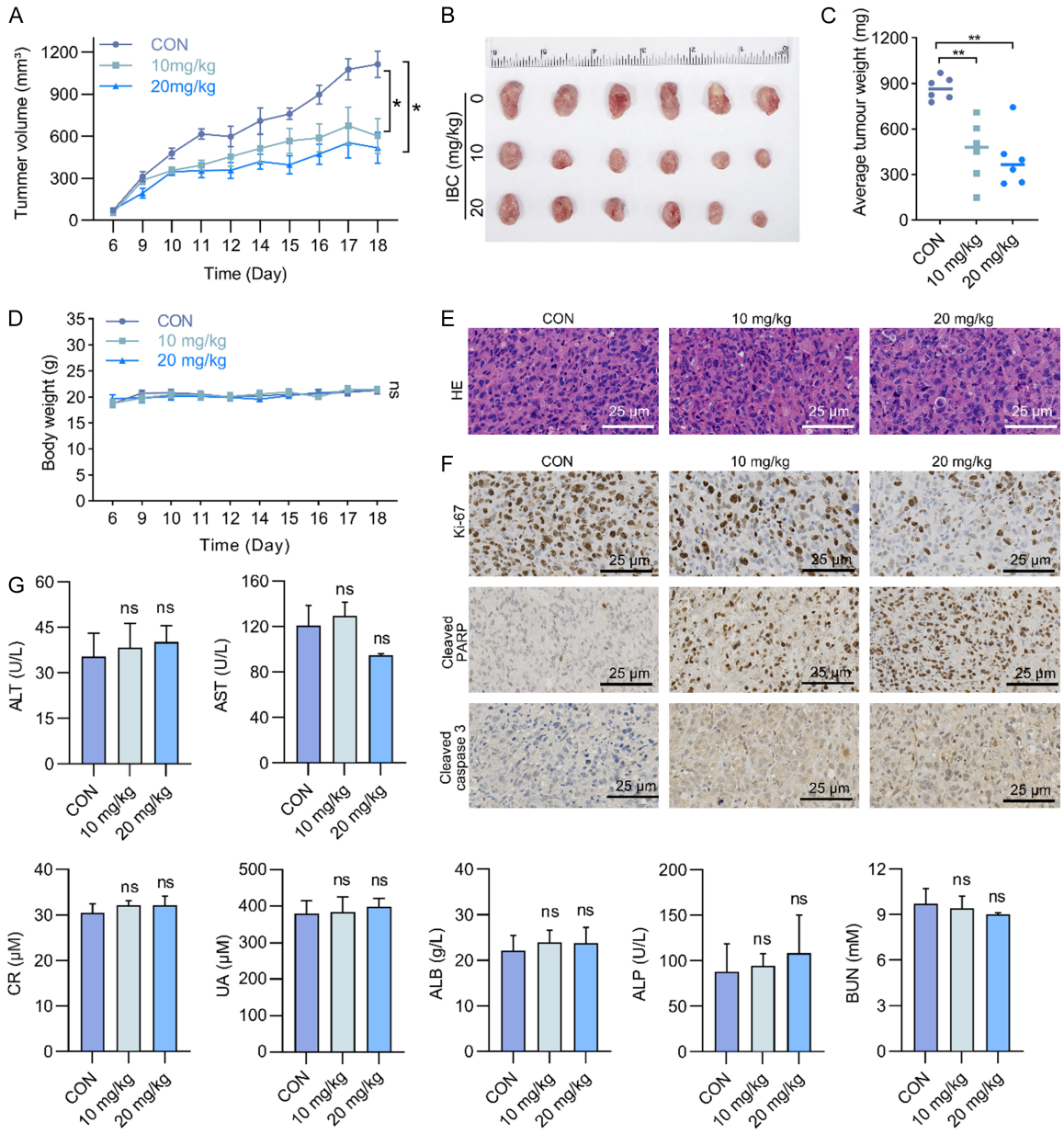

Figure 4. IBC inhibits ATC xenograft growth in nude mice. (A) Tumor growth curves of 8505C xenografts in BALB/c nude mice treated with IBC (0 mg/kg, 10 mg/kg and 20 mg/kg, intraperitoneal injection, n = 6). Tumor volumes were monitored every other day (mean ± SD). (B) Macroscopic views and average weights (mean ± SD) of the excised tumors at the endpoint are also shown (C). (D) Body weights of the mice were recorded every other day throughout the study (mean ± SD). (E) Representative H&E-stained images of the xenograft tumor tissues. (F) Expression of Ki67, cleaved-caspase 3, and cleaved-PARP in xenograft tumors was assessed by immunohistochemistry (IHC). (G) Liver and kidney function indicators (ALT, AST, CR, UA, ALB, ALP, and BUN) were measured in BALB/c nude mice. Values are presented as mean ± SD for n = 3. **P < 0.01.

ed in several solid tumors, including lung cancer and melanoma, contributing to tumor immune escape [36-39]. Conversely, activation of GSDME-dependent pyroptosis can enhance the therapeutic efficacy of immune checkpoint inhibitors, such as anti-PD-1 antibodies [40-42]. Studies have shown that ATC exhibits high GSDME expression [33], therapies inducing GSDME-mediated pyroptosis could be particularly effective against this tumor type. Although our results show that IBC effectively inhibits tumor growth in ATC subcutaneous xenografts in nude mice, its anticancer effects need to be further evaluated in immunocompetent ATC

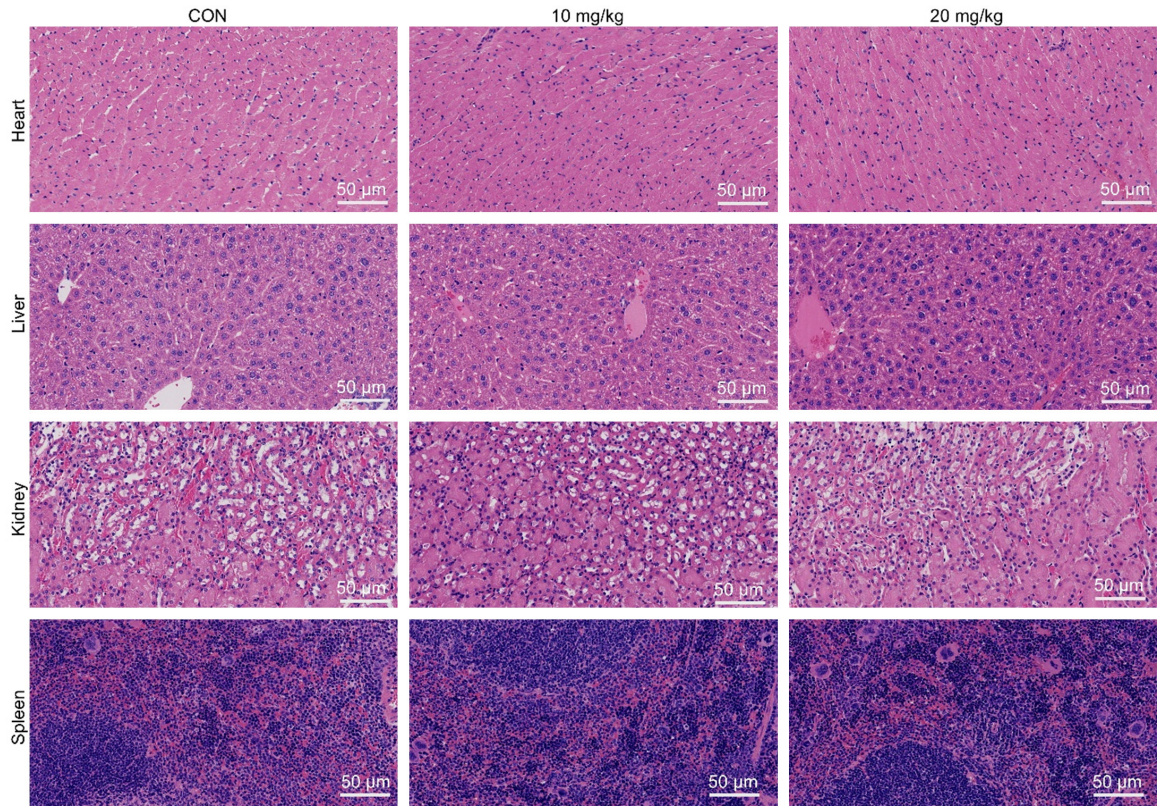

Figure 5. Histopathological evaluation of major organs from IBC-treated mice. Representative H&E-stained sections of the heart, liver, kidney, and spleen from control and IBC-treated mice (10 and 20 mg/kg) at the study endpoint. No overt histopathological abnormalities or treatment-related lesions were observed across groups. Scale bar = 50 μm (applies to all images).

models to determine potential immune-mediated mechanisms. Given that IBC induces pyroptosis in ATC cells and promotes the release of factors such as IL-1β, we believe it holds potential to modulate the tumor immune microenvironment and enhance antitumor responses.

Conclusion

In summary, this study demonstrates that IBC effectively suppresses ATC tumor growth both *in vitro* and *in vivo*. IBC inhibits ATC cells growth and colony formation, induces cell cycle arrest, and triggers apoptosis and pyroptosis, with caspase-3-mediated PARP cleavage and GSDME activation. Notably, IBC exhibited minimal toxicity in mice. These findings highlight IBC as a promising therapeutic candidate and a potential strategy for treating ATC.

Acknowledgements

This work was supported by grants from the National Natural Science Foundation of China (82372618, 82573843); the Natural Science Foundation of Zhejiang Province (LY23H160024); Medical Health Science and Technology Project of Zhejiang Provincial Health Commission (2024KY034).

Disclosure of conflict of interest

None.

Address correspondence to: Minghua Ge and Guowan Zheng, Otolaryngology & Head and Neck Center, Cancer Center, Department of Head and Neck Surgery, Zhejiang Provincial People's Hospital (Affiliated People's Hospital), Hangzhou Medical College, 158 Shangtang Road, Hangzhou 310014, Zhejiang, China. E-mail: geminghua@hmc.edu.cn (MHG); zhengguowan@hmc.edu.cn (GWZ)

References

[1] Jannin A, Escande A, Al Ghuzlan A, Blanchard P, Hartl D, Chevalier B, Deschamps F, Lamartina L, Lacroix L, Dupuy C, Baudin E, Do Cao C

and Hadoux J. Anaplastic thyroid carcinoma: an update. Cancers (Basel) 2022; 14: 1061.
[2] Wang M, Lin L, Lu JJ and Chen X. Pharmacological review of isobavachalcone, a naturally occurring chalcone. Pharmacol Res 2021; 165: 105483.
[3] Li S, Chen X, Shi H, Yi M, Xiong B and Li T. Tailoring traditional Chinese medicine in cancer therapy. Mol Cancer 2025; 24: 27.
[4] Xing N, Meng X and Wang S. Isobavachalcone: a comprehensive review of its plant sources, pharmacokinetics, toxicity, pharmacological activities and related molecular mechanisms. Phytother Res 2022; 36: 3120-3142.
[5] Li Y, Qin X, Li P, Zhang H, Lin T, Miao Z and Ma S. Isobavachalcone isolated from *Psoralea corylifolia* inhibits cell proliferation and induces apoptosis via inhibiting the AKT/GSK-3beta/beta-catenin pathway in colorectal cancer cells. Drug Des Devel Ther 2019; 13: 1449-1460.
[6] Li K, Zheng Q, Chen X, Wang Y, Wang D and Wang J. Isobavachalcone induces ROS-mediated apoptosis *via* targeting thioredoxin reductase 1 in human prostate cancer PC-3 cells. Oxid Med Cell Longev 2018; 2018: 1915828.
[7] Ren YL, Lei JT, Zhang TR, Lu P, Cui DD, Yang B, Zhao GY, Peng F, Cao ZX, Peng C and Li YZ. Isobavachalcone, a natural sirtuin 2 inhibitor, exhibits anti-triple-negative breast cancer efficacy in vitro and in vivo. Phytother Res 2024; 38: 1815-1829.
[8] Chen J, Zhao L, Xu MF, Huang D, Sun XL, Zhang YX, Li HM and Wu CZ. Novel isobavachalcone derivatives induce apoptosis and necroptosis in human non-small cell lung cancer H1975 cells. J Enzyme Inhib Med Chem 2024; 39: 2292006.
[9] Liu X, Zhang H, Cao J, Zhuo Y, Jin J, Gao Q, Yuan X, Yang L, Li D and Wang Y. Isobavachalcone activates antitumor immunity on orthotopic pancreatic cancer model: a screening and validation. Front Pharmacol 2022; 13: 919035.
[10] Tong X, Tang R, Xiao M, Xu J, Wang W, Zhang B, Liu J, Yu X and Shi S. Targeting cell death pathways for cancer therapy: recent developments in necroptosis, pyroptosis, ferroptosis, and cuproptosis research. J Hematol Oncol 2022; 15: 174.
[11] Vande Walle L and Lamkanfi M. Author correction: drugging the NLRP3 inflammasome: from signalling mechanisms to therapeutic targets. Nat Rev Drug Discov 2025; 24: 72.
[12] Bertheloot D, Latz E and Franklin BS. Necroptosis, pyroptosis and apoptosis: an intricate game of cell death. Cell Mol Immunol 2021; 18: 1106-1121.
[13] Shi J, Zhao Y, Wang Y, Gao W, Ding J, Li P, Hu L and Shao F. Inflammatory caspases are innate immune receptors for intracellular LPS. Nature 2014; 514: 187-192.
[14] Du T, Gao J, Li P, Wang Y, Qi Q, Liu X, Li J, Wang C and Du L. Pyroptosis, metabolism, and tumor immune microenvironment. Clin Transl Med 2021; 11: e492.
[15] Wang H, Wang T, Yan S, Tang J, Zhang Y, Wang L, Xu H and Tu C. Crosstalk of pyroptosis and cytokine in the tumor microenvironment: from mechanisms to clinical implication. Mol Cancer 2024; 23: 268.
[16] Hanggi K and Ruffell B. Cell death, therapeutics, and the immune response in cancer. Trends Cancer 2023; 9: 381-396.
[17] Liang T, Gu L, Kang X, Li J, Song Y, Wang Y and Ma W. Programmed cell death disrupts inflammatory tumor microenvironment (TME) and promotes glioblastoma evolution. Cell Commun Signal 2024; 22: 333.
[18] Wang Y, Gao W, Shi X, Ding J, Liu W, He H, Wang K and Shao F. Chemotherapy drugs induce pyroptosis through caspase-3 cleavage of a gasdermin. Nature 2017; 547: 99-103.
[19] Yuan J and Ofengeim D. A guide to cell death pathways. Nat Rev Mol Cell Biol 2024; 25: 379-395.
[20] Liu Y, Pan R, Ouyang Y, Gu W, Xiao T, Yang H, Tang L, Wang H, Xiang B and Chen P. Pyroptosis in health and disease: mechanisms, regulation and clinical perspective. Signal Transduct Target Ther 2024; 9: 245.
[21] Hu Y, Wen Q, Cai Y, Liu Y, Ma W, Li Q, Song F, Guo Y, Zhu L, Ge J, Zeng Q, Wang J, Yin C, Zheng G and Ge M. Alantolactone induces concurrent apoptosis and GSDME-dependent pyroptosis of anaplastic thyroid cancer through ROS mitochondria-dependent caspase pathway. Phytomedicine 2023; 108: 154528.
[22] Liu Y, Guo Y, Zeng Q, Hu Y, He R, Ma W, Qian C, Hua T, Song F, Cai Y, Zhu L, Ren X, Xu J, Zheng C, Ding L, Ge J, Wang W, Xu H, Ge M and Zheng G. Prosapogenin A induces GSDME-dependent pyroptosis of anaplastic thyroid cancer through vacuolar ATPase activation-mediated lysosomal over-acidification. Cell Death Dis 2024; 15: 586.
[23] Guo YW, Zhu L, Duan YT, Hu YQ, Li LB, Fan WJ, Song FH, Cai YF, Liu YY, Zheng GW and Ge MH. Ruxolitinib induces apoptosis and pyroptosis of anaplastic thyroid cancer via the transcriptional inhibition of DRP1-mediated mitochondrial fission. Cell Death Dis 2024; 15: 125.
[24] Cao D, Zhang Z, Jiang X, Wu T, Xiang Y, Ji Z, Guo J, Zhang X, Xu K, Liu Z and Zhang Y. Psoralea corylifolia L. and its active component isobavachalcone demonstrate antibacterial activity against Mycobacterium abscessus. J Ethnopharmacol 2024; 329: 118142.
[25] Li B, Xu N, Wan Z, Ma L, Li H, Cai W, Chen X, Huang Z and He Z. Isobavachalcone exerts

anti-proliferative and pro-apoptotic effects on human liver cancer cells by ta-rgeting the ERKs/RSK2 signaling pathway. Oncol Rep 2019; 41: 3355-3366.
[26] Zhang Y, Gao M, Zhu M, Li H, Ma T and Wu C. Isobavachalcone induces cell death through multiple pathways in human breast cancer MCF-7 cells. Nan Fang Yi Ke Da Xue Xue Bao 2022; 42: 878-885.
[27] Wei X, Xie F, Zhou X, Wu Y, Yan H, Liu T, Huang J, Wang F, Zhou F and Zhang L. Role of pyroptosis in inflammation and cancer. Cell Mol Immunol 2022; 19: 971-992.
[28] Bhardwaj A, Panepinto MC, Ueberheide B and Neel BG. A mechanism for hypoxia-induced inflammatory cell death in cancer. Nature 2025; 637: 470-477.
[29] Fontana P, Du G, Zhang Y, Zhang H, Vora SM, Hu JJ, Shi M, Tufan AB, Healy LB, Xia S, Lee DJ, Li Z, Baldominos P, Ru H, Luo HR, Agudo J, Lieberman J and Wu H. Small-molecule GSDMD agonism in tumors stimulates antitumor immunity without toxicity. Cell 2024; 187: 6165-6181, e6122.
[30] Loveless R, Bloomquist R and Teng Y. Pyroptosis at the forefront of anticancer immunity. J Exp Clin Cancer Res 2021; 40: 264.
[31] Bhat AA, Thapa R, Afzal O, Agrawal N, Almalki WH, Kazmi I, Alzarea SI, Altamimi ASA, Prasher P, Singh SK, Dua K and Gupta G. The pyroptotic role of Caspase-3/GSDME signalling pathway among various cancer: a review. Int J Biol Macromol 2023; 242: 124832.
[32] Jiang M, Qi L, Li L and Li Y. The caspase-3/GSDME signal pathway as a switch between apoptosis and pyroptosis in cancer. Cell Death Discov 2020; 6: 112.
[33] Zhang Z, Zhang Y, Xia S, Kong Q, Li S, Liu X, Junqueira C, Meza-Sosa KF, Mok TMY, Ansara J, Sengupta S, Yao Y, Wu H and Lieberman J. Gasdermin E suppresses tumour growth by activating anti-tumour immunity. Nature 2020; 579: 415-420.
[34] Christgen S, Tweedell RE and Kanneganti TD. Programming inflammatory cell death for therapy. Pharmacol Ther 2022; 232: 108010.
[35] Gao W, Wang X, Zhou Y, Wang X and Yu Y. Autophagy, ferroptosis, pyroptosis, and necroptosis in tumor immunotherapy. Signal Transduct Target Ther 2022; 7: 196.
[36] Dong X, Nie J, Huang A, Chen L, Zang E, Xiang Z, Hao X, Yan S, Ding X and Zhao Y. A novel small molecule NJH-13 induces pyroptosis via the Ca(2+) driven AKT-FOXO1-GSDME signaling pathway in NSCLC by targeting TRPV5. J Adv Res 2025; 77: 733-746.
[37] Ibrahim J, Op de Beeck K, Fransen E, Croes L, Beyens M, Suls A, Vanden Berghe W, Peeters M and Van Camp G. Methylation analysis of Gasdermin E shows great promise as a biomarker for colorectal cancer. Cancer Med 2019; 8: 2133-2145.
[38] Xia Y, Jin Y, Cui D, Wu X, Song C, Jin W and Huang H. Antitumor effect of simvastatin in combination with DNA methyltransferase inhibitor on gastric cancer via GSDME-mediated pyroptosis. Front Pharmacol 2022; 13: 860546.
[39] Zhao P, Wang M, Chen M, Chen Z, Peng X, Zhou F, Song J and Qu J. Programming cell pyroptosis with biomimetic nanoparticles for solid tumor immunotherapy. Biomaterials 2020; 254: 120142.
[40] Enssle S, Sax A, May P, El Khawanky N, Soliman N, Perl M, Enssle JC, Krey K, Ruland J, Pichlmair A, Bassermann F, Poeck H and Heidegger S. Gasdermin E links tumor cell-intrinsic nucleic acid signaling to proinflammatory cell death for successful checkpoint inhibitor cancer immunotherapy. Oncoimmunology 2025; 14: 2504244.
[41] Zhou Y, Zhang W, Wang B, Wang P, Li D, Cao T, Zhang D, Han H, Bai M, Wang X, Zhao X and Lu Y. Mitochondria-targeted photodynamic therapy triggers GSDME-mediated pyroptosis and sensitizes anti-PD-1 therapy in colorectal cancer. J Immunother Cancer 2024; 12: e008054.
[42] Gao Q, Sheng Q, Yang Z, Zhu Z, Li L, Xu L, Xia J, Qiao Y, Gu J, Zhu X, Xie T and Sui X. Honokiol-Magnolol-Baicalin possesses synergistic anticancer potential and enhances the efficacy of anti-PD-1 immunotherapy in colorectal cancer by triggering GSDME-dependent pyroptosis. Adv Sci (Weinh) 2025; 12: e2417022.